



Holocene atmospheric circulation in the central North Pacific: A new terrestrial diatom and $\delta^{18}\text{O}$ dataset from the Aleutian Islands

Hannah L. Bailey ^{a, b, c, *}, Darrell S. Kaufman ^d, Hilary J. Sloane ^e, Alun L. Hubbard ^f, Andrew C.G. Henderson ^g, Melanie J. Leng ^{e, h}, Hanno Meyer ^b, Jeffrey M. Welker ^{a, c}

^a Department of Biological Sciences, University of Alaska Anchorage, Anchorage, AK 99508, USA

^b Alfred Wegener Institute for Polar and Marine Research, Potsdam, 14473, Germany

^c Department of Ecology and Genetics, University of Oulu, Oulu, Finland

^d School of Earth Sciences & Environmental Sustainability, Northern Arizona University, Flagstaff, AZ 86011, USA

^e NERC Isotope Geosciences Facility, British Geological Survey, Nottingham, NG12 5GG, UK

^f Centre for Arctic Gas Hydrate, Environment and Climate, Department of Geology, UiT The Arctic University of Norway, 9037 Tromsø, Norway

^g School of Geography, Politics and Sociology, Newcastle University, Newcastle-upon-Tyne, NE7 1RU, UK

^h Centre for Environmental Geochemistry, School of Biosciences, University of Nottingham, Loughborough, LE12 5RD, UK

ARTICLE INFO

Article history:

Received 7 May 2018

Received in revised form

27 June 2018

Accepted 27 June 2018

Keywords:

Holocene

Paleoclimate

North Pacific

Limnology

Stable isotopes

Diatoms

ABSTRACT

The North Pacific is a zone of cyclogenesis that modulates synoptic-scale atmospheric circulation, yet there is a paucity of instrumental and paleoclimate data to fully constrain its long-term state and variability. We present the first Holocene oxygen isotope record ($\delta^{18}\text{O}_{\text{diatom}}$) from the Aleutian Islands, using siliceous diatoms preserved in Heart Lake on Adak Island (51.85° N, 176.69° W). This study builds on previous work demonstrating that Heart Lake sedimentary $\delta^{18}\text{O}_{\text{diatom}}$ values record the $\delta^{18}\text{O}$ signal of precipitation, and correlate significantly with atmospheric circulation indices over the past century. We apply this empirical relationship to interpret a new 9.6 ka $\delta^{18}\text{O}_{\text{diatom}}$ record from the same lake, supported by diatom assemblage analysis. Our results demonstrate distinct shifts in the prevailing trajectory of storm systems that drove spatially heterogeneous patterns of moisture delivery and climate across the region. During the early-mid Holocene, a warmer/wetter climate prevailed due to a predominantly westerly Aleutian Low that enhanced advection of warm ^{18}O -enriched Pacific moisture to Adak, and culminated in a $\delta^{18}\text{O}_{\text{diatom}}$ maxima (33.3‰) at 7.6 ka during the Holocene Thermal Maximum. After 4.5 ka, relatively lower $\delta^{18}\text{O}_{\text{diatom}}$ indicates cooler/drier conditions associated with enhanced northerly circulation that persisted into the 21st century. Our analysis is consistent with surface climate conditions inferred from a suite of terrestrial and marine climate-proxy records. This new Holocene dataset bridges the gap in an expanding regional network of paleoisotope studies, and provides a fresh assessment of the complex spatial patterns of Holocene climate across Beringia and the atmospheric forces driving them.

© 2018 Elsevier Ltd. All rights reserved.

1. Introduction

Numerous paleoenvironmental studies now contribute to a global synthesis and understanding of Holocene climate change over the past 11.7 ka (Mayewski et al. 2004; Marcott et al. 2013; Rehfeld et al. 2018). By comparing common trends between individual proxy records, these studies provide a means to infer the timing, scale, and spatial extent of major Holocene climatic

features. These include stepwise climate transitions, intervals exceeding twentieth century warmth, and the low-frequency behaviour and modes of natural climate variability. At broad (i.e. global) spatial and temporal scales these trends are relatively coherent and unambiguous, yet at finer spatial scales, climate variability is more pronounced due to local and regional factors. Such variability is highlighted in two recent paleoclimate syntheses focused on west and eastern Beringia – the region extending from northeast Siberia to northwest Canada (Fig. 1a) (Brooks et al. 2015; Kaufman et al. 2016). While general circulation models (GCM) typically emphasise insolation as the key driver of millennial-scale Holocene climate change (Renssen et al. 2009), these compilations indicate a more complex and spatially heterogeneous climate

* Corresponding author. Department of Ecology and Genetics, University of Oulu, Oulu, Finland.

E-mail address: Hannah.Bailey@oulu.fi (H.L. Bailey).

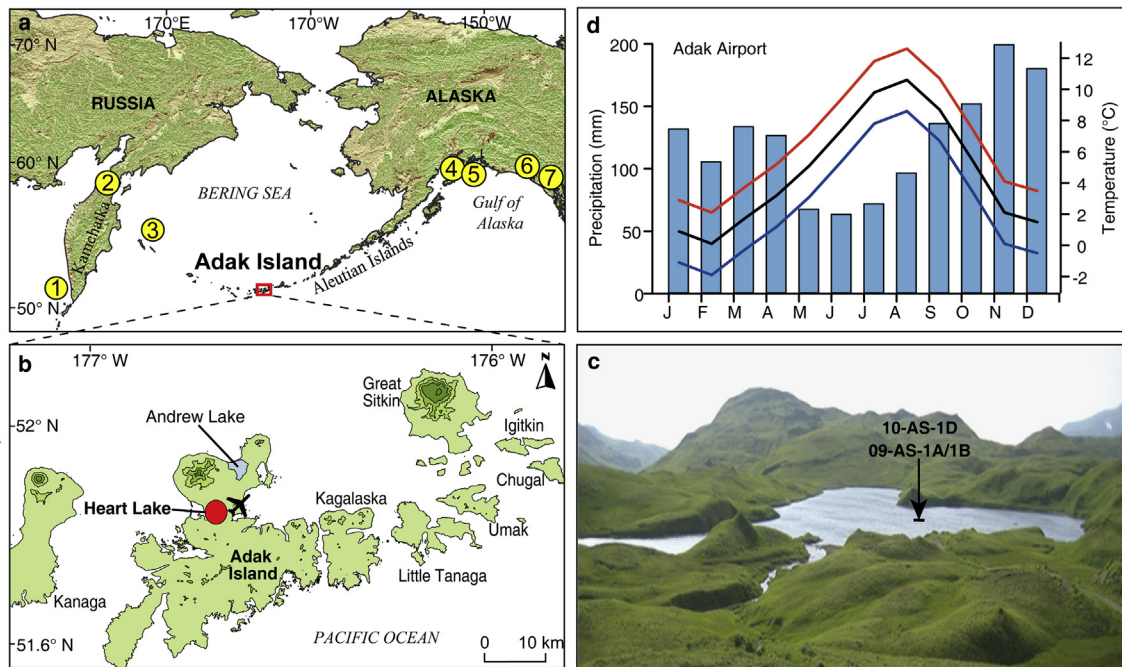


Fig. 1. Location of (a) Adak Island in the central Aleutian Islands, (b) Heart Lake and Andrew Lake, (c) oblique north west view of Heart Lake with the inflow channel visible in the foreground [credit: Yarrow Axford], and (d) monthly mean precipitation (blue bars) and surface air temperature at Adak airport (1949–2016), whereby solid lines depict mean (black), minimum (blue) and maximum (red) temperatures (NOAA, 2017). Numbered circles in 1a indicate key sites referred to in text: (1) LV29-114-3 (Max et al. 2012), (2) Pechora Lake (Hammarlund et al. 2015), (3) SO201-12-77KL (Max et al. 2012), (4) Horse Trail Fen (Jones et al. 2014), (5) Mica Lake (Schiff et al. 2009), (6) Mount Logan (Fisher et al. 2008), and (7) Jellybean Lake (Anderson et al. 2005). (For interpretation of the references to colour in this figure legend, the reader is referred to the Web version of this article.)

evolution than implied by linear insolation forcing alone. For example, major climatic features previously considered ubiquitous, such as a prominent Holocene thermal maximum (HTM) (Kaufman et al. 2004), are now recognised to be spatially asynchronous across this vast region (Kaufman et al. 2016). Moreover, existing terrestrial water isotope records are also shown to be ambiguous and contradictory during the Holocene (Kaufman et al. 2016), and the most recent suite of model-data comparisons reveal significant mismatches between simulated and reconstructed Holocene temperatures in Alaska (Zhang et al. 2017).

At the synoptic scale, Beringia is located within the main centre of influence of the Aleutian Low; one of the most dominant ocean-atmospheric systems in the Northern Hemisphere and of global climate significance (Rodionov et al. 2007). However, virtually all available terrestrial paleoclimate data are restricted to mainland Alaska and eastern Russia (Sundqvist et al. 2014; Brooks et al. 2015; Kaufman et al. 2016), and compared to lower latitude regions, paleoisotope reconstructions are sparse (Kaufman et al. 2016). This partly reflects a lack of base-line water isotope measurements for constraining the regional water isotope cycle [e.g. Welker, 2000; Anderson et al. 2016], as well as a paucity of lake core studies with continuous sequences of carbonate-rich sediments – or suitable alternatives – for isotopic analysis. Hence, to elucidate past and future climate in this region, there is an outstanding requirement for greater spatial coverage of highly resolved and accurately dated paleoclimate datasets, as well as an empirical-based understanding of the atmospheric and environmental controls driving them.

To address this, we present the first Holocene oxygen isotope record from the Aleutian Islands in south west Alaska. Our isotope measurements derive from siliceous diatoms ($\delta^{18}\text{O}_{\text{diatom}}$) preserved in the sediments of Heart Lake, on Adak Island (Fig. 1b), and are supported by diatom assemblage analysis of the same sedimentary sequence. We build on earlier work by Bailey et al. (2015) who demonstrate that Heart Lake $\delta^{18}\text{O}_{\text{diatom}}$ values correlate

significantly with North Pacific climate indices over the past hundred years ($r = 0.43$; $p < 0.02$, $n = 28$). Here, we apply this empirically-derived understanding to interpret new $\delta^{18}\text{O}_{\text{diatom}}$ data from a longer Heart Lake sediment core which extends back to 9.6 ka. The primary aims are to: (1) investigate the forcing and response of this remote region to a warming climate system as it transitioned from the last glacial period; (2) develop a Holocene reconstruction of North Pacific atmospheric circulation; and (3) bridge the gap in the regional network of proxy records to synthesise and assess complex spatio-temporal patterns of natural climate variability across Beringia.

2. Regional setting

Heart Lake is a small ($\sim 0.25 \text{ km}^2$), freshwater through-flow system on Adak Island in the central North Pacific (51.85° N , 176.69° W) (Fig. 1c). The island is volcanic and forms part of the 1900-km-long Aleutian archipelago extending from mainland Alaska to the Russian-Kamchatka Peninsula. The lake watershed area is $\sim 8 \text{ km}^2$ and is situated in low-relief hills surrounded by mountainous terrain (Fig. 1c). There is a single lake basin with a maximum depth of 8 m. One stream inflows from two larger lakes and a small outflow channel drains to the Bering Sea $\sim 2 \text{ km}$ to the west. Lake volume is $\sim 8 \times 10^5 \text{ m}^3$ and water retention is an estimated two weeks, based on the available stream gauge inflow data (TDX, 2013). Inspection of available satellite imagery reveals that Heart Lake freezes over in winter and this ice surface remains into spring (USGS, 2017).

Adak Island has a mild maritime climate compared to mainland Alaska and is strongly affected by persistent fog and light rain in the summer, and frequent storms and strong winds during winter (Rodionov et al. 2007). Mean annual air temperature is 4.3° C , and mean winter (December–February) and summer (June–August) values are 1.0° C and 9.0° C , respectively (1949–2016) (NOAA,

2017). Mean December and July precipitation is 163 mm and 71 mm, respectively (Fig. 1d) (NOAA, 2017). Of the total 1.3 m annual precipitation, ~75% (1.0 m) falls from September to February.

The regional climate reflects the configuration of large scale atmospheric–ocean systems, namely the Aleutian Low: a synoptic-scale feature of mean low sea level pressure (SLP) and the leading driver of North Pacific climate (Mock et al. 1998). When the Aleutian Low is ‘weak’, storms tend to track north over the central Aleutian Islands (Fig. 2a); when the pressure system is ‘strong’, storms track south of the Aleutians and into the Gulf of Alaska (Fig. 2b) (Mock et al. 1998; Rodionov et al. 2007). These circulation patterns vary on interannual to decadal timescales and induce characteristic climate responses that are well expressed in coupled modes of the North Pacific Index (NPI) and the Pacific Decadal Oscillation (PDO) (Trenberth and Hurrell, 1994; Mantua et al. 1997). Typically, a strong Aleutian Low (–NPI/+PDO) will induce positive sea surface temperatures (SST), surface air temperatures (SAT), and precipitation anomalies in the Gulf of Alaska and negative anomalies in the central North Pacific, with contrary conditions during a weak Aleutian Low (+NPI/–PDO) (see Supplementary Fig. 1).

3. Materials and methods

3.1. Sediment and water recovery

Sediment cores and bottom lake water samples were recovered

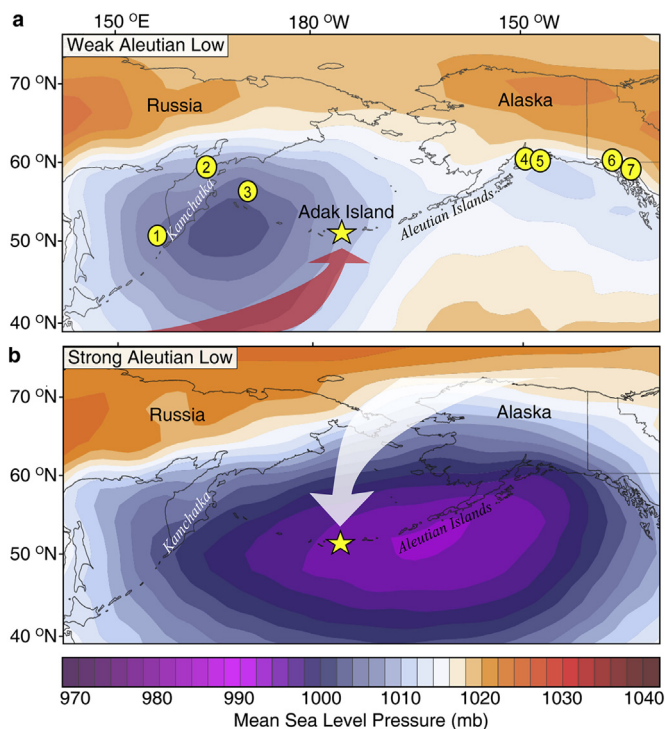


Fig. 2. Mean winter (December–February) sea level pressure associated with the six most positive (a) and negative (b) North Pacific Index (NPI) values between 1950 and 2017 (Trenberth and Hurrell, 1994). A negative (positive) NPI is a strong (weak) Aleutian Low. Arrows highlight the direction of the primary storm tracks delivering precipitation to our site on Adak Island (yellow star) (Bailey et al. 2015). SLP data obtained from NCEP/NCAR V1 reanalysis (Kalnay et al. 1996). Numbered yellow circles in (a) indicate locations of the (1) LV29-114-3 (Max et al. 2012), (2) Pechora Lake (Hammarlund et al. 2015), (3) SO201-12-77KL (Max et al. 2012), (4) Horse Trail Fen (Jones et al. 2014), (5) Mica Lake (Schiff et al. 2009), (6) Mount Logan (Fisher et al. 2008), and (7) Jellybean Lake (Anderson et al. 2005) climate records discussed in text. (For interpretation of the references to colour in this figure legend, the reader is referred to the Web version of this article.)

from Heart Lake during the summers of 2009 and 2010. A Garmin GPS sonar was used to survey its bathymetry and revealed a single basin with a maximum depth of 8 m, surrounded by a shallow platform <2 m deep (see Supplementary Fig. 2). Coring sites were selected adjacent to the deepest part of the basin at a depth of 7.6 m. Seven sediment cores were extracted using percussion and hand-held gravity coring devices operated from a floating platform. Bottom lake water samples were collected *in situ* at the sediment-water interface during gravity coring. Following core extraction the water was directly siphoned from the corer and sealed in 50 ml vials, ensuring no head space. Sediment cores were then split lengthways, packaged, and shipped with water samples to Northern Arizona University where they were stored at 4 °C until they were sub-sampled and analyzed. Our study focuses on the longest percussion core (10-AS-1D; 5.9 m) and two accompanying surface gravity cores (09-AS-1A, 0.81 m; and 09-AS-1B, 0.44 m). For a detailed description of the sediment core's lithostratigraphy, see Krawiec et al. (2013).

3.2. Chronology

The composite age model for 10-AS-1D and 09-AS-1A is presented in a separate paper devoted to the tephrostratigraphy and radiometric dating of the Heart Lake sedimentary sequence (Krawiec et al. 2013) (Supplementary Fig. 3a). In summary, a Monte Carlo approach was employed to model the age–depth relation of 16 macrofossil AMS radiocarbon (^{14}C) dates, together with a peak in recent $^{239+240}\text{Pu}$ activity and the age of the sediment–water interface (2009 AD) (Krawiec et al. 2013). Tephrostratigraphy was used to independently cross check the accuracy of the chronology, whereby the ages of down core tephra horizons from Heart Lake were compared with tephra ages from nearby Andrew Lake and previously published outcrop studies (Krawiec et al. 2013). The chronology for surface core 09-AS-1B derives from radiometric dating of ^{210}Pb , ^{226}Ra , ^{137}Cs and ^{241}Am by direct gamma assay on 14 dried sediment samples from the upper core section (Bailey et al. 2015) (Supplementary Fig. 3b). The cores were cross-correlated using a prominent tephra horizon found in all three sedimentary sequences (Krawiec et al. 2013; Bailey et al. 2015). All ages herein are expressed as thousands of calendar years (ka) prior to 1950 AD, where 1 ka = 1000 cal yr BP.

3.3. Stable isotope analyses

A total of 147 sediment samples were processed for $\delta^{18}\text{O}_{\text{diatom}}$ analysis. These samples range in age from 9.6 ka (587 cm depth) to 2009 AD, and are sub-/decadally resolved for the most recent 1500 years and at centennial resolution thereafter. From the 5.9 m-long core 10-AS-1D, 1 cm³ of sediment was extracted at 7 cm intervals from the base (587 cm) to the top of the core. This was the optimal sampling resolution to avoid tephra layers which could potentially cause contamination issues (Lamb et al. 2007). The surface cores 09-AS-1A and 09-AS-1B were both sampled in contiguous 0.5 cm increments. This detail was used to capture sub-decadal changes in $\delta^{18}\text{O}_{\text{diatom}}$ over the past century for direct comparison with instrumental datasets (see Bailey et al. 2015).

Sediment samples were prepared using a hybrid process of chemical digestion, sieving, and heavy liquid separation adapted from Morley et al. (2004). To remove organic and carbonate material, samples were treated with 30% H_2O_2 at 90 °C until reactions ceased, before using 5% HCl at ambient temperature. Samples were then centrifuged in sodium polytungstate ($3\text{Na}_2\text{WO}_4 \cdot 9\text{H}_2\text{O}$) (SPT) heavy liquid at 2500 rpm for 20 min, resulting in the separation and suspension of diatoms from the heavier detritus. This procedure was repeated three times for each sample using specific

gravities of 2.50, 2.30 and 2.25 g ml⁻¹. After the final SPT separation, samples were washed five times in ultrapure water (UPW) at 1500 rpm for 5 min and vacuum filtered through a 3 µm cellulose nitrate membrane to remove potential clay minerals and/or broken diatom fragments. The <3 µm fraction was discarded as it was too small (<1 mg) to be analyzed and, upon further inspection under a light microscope, contained only small broken diatom fragments and detritus. The remaining samples were treated with a final stage of 30% H₂O₂ at 60 °C for one week to ensure no traces of organic matter remained.

Purified diatom samples were analyzed for δ¹⁸O_{diatom} using the stepwise fluorination method (Leng and Sloane, 2008) at the NERC Isotope Geosciences Laboratory in Keyworth, UK. The outer hydrous layer of the diatom was removed in a pre-fluorination stage using a BrF₅ reagent at low temperature (Leclerc and Labeyrie, 1987). This was followed by a full reaction at high temperature to liberate oxygen that was converted to CO₂ (Clayton and Mayeda, 1963) and measured for δ¹⁸O_{diatom} using a MAT 253 dual-inlet mass spectrometer. Replicate analyses indicate an analytical reproducibility of ±0.19‰ (1σ) for the samples, and ±0.30‰ (1σ) for the diatom standard BFC_{mod}. All δ¹⁸O values were converted to the Vienna Standard Mean Ocean Water (VSMOW) scale using the BFC_{mod} standard for calibration.

Two Heart Lake water samples were measured for their oxygen and hydrogen (δD) isotope composition using a Thermo-Finnigan Deltaplus XL gas mass spectrometer at the Colorado Plateau Stable Isotope Laboratory, Northern Arizona University, USA. Analytical precision on internal working standards was ±0.1‰ for δ¹⁸O and ±1‰ for δD. All values are reported here in per mil (‰) relative to VSMOW.

3.3.1. Contamination assessment

All purified diatom samples (n = 147) were visually inspected for contamination using an OLYMPUS BX40 light microscope. Thirty samples were selected down-core and further inspected using a Hitachi S-4700 field emission scanning electron microscope (SEM). In addition, fourier transform infrared spectroscopy (FTIR) was applied to assess the chemical composition and sample purity of 16 diatom samples from core 10-AS-1D (Swann and Patwardhan, 2011). These samples, together with the BFC_{mod} diatom standard, were analyzed using FTIR at the British Geological Survey in Keyworth, UK (Bailey et al. 2014). FTIR analyses of all purified diatom isotope samples measured (n = 16) indicate peaks corresponding to the BFC_{mod} standard, known to represent clean, fossilised diatomite (Supplementary Fig. 4). Spectral deviation from the standard would indicate additional compounds and contamination by non-diatom components (Swann and Patwardhan, 2011); peaks centred at ~450 cm⁻¹, ~800 cm⁻¹ and ~1100 cm⁻¹ confirm pure silica and the integrity of our diatom isotope samples (Bailey et al. 2014).

3.4. Diatom assemblage analysis

Fifty-seven sub-samples of the purified diatom material used for δ¹⁸O_{diatom} analysis were retained for diatom species analysis. These include 33 samples selected at c. 13 cm intervals from AS-10-1D, and 24 samples at a contiguous 0.5 cm resolution from AS-09-1B. Diatom slides were prepared on a hot plate using Naphrax[®] mounting medium. A minimum of 300 diatom frustules per sample were counted along transects at ×1000 magnification, under an OLYMPUS B×40 light microscope. Taxonomic identification was based on classifications in Camburn and Charles (2000) and Krammer and Lange-Bertalot (1986–1991).

Following diatom identification, species counts were converted to percentage abundance and evaluated using the software package Tilia (v.2.0.41) (Grimm, 2015). For diatom zone demarcation, a

constrained incremental sum-of-squares cluster analysis (CONISS) (Grimm, 1987) was applied to all dominant taxa with a relative abundance >5% in at least one sample. To quantitatively assess the down core trends in diatom assemblages, a principal components analysis (PCA) (ter Braak and Prentice, 1988) was applied to a correlation matrix based on the dominant (>5%) diatom species in all 57 samples. The analysis was performed on untransformed percentage data using the program C2 (v.1.7.6) (Juggins, 2014).

4. Results

4.1. Diatom flora

Diatom frustules are well preserved in all samples and show no sign of valve dissolution. The flora is diverse and a total of 155 different freshwater diatom species were identified. Of these, 11 species account for >90% of all diatoms present in all samples. These include species belonging to the genera *Aulacoseira*, *Cyclotella*, *Rossithidium*, and small fragilarioid taxa (consisting of the genera *Fragilaria*, *Pseudostaurosira*, *Staurosira*, *Stauroforma*, and *Staurosirella*). Species with an abundance ≥5% in at least one stratigraphic level are presented (Fig. 3), and the record is divided into four zones based on the CONISS dendrogram: Zone 1 (9.6–8.6 ka; 587–452 cm), Zone 2 (8.6–4.4 ka; 452–352 cm), Zone 3 (4.4 ka–1860 AD; 352–13.25 cm), and Zone 4 (1860–2009 AD; 13.25–0 cm). Species are grouped into one of three habitat types (planktonic, benthic, or facultatively planktonic) based on classifications by Spaulding et al. (2017) (Fig. 3).

Diatom Zone 1 (587–452 cm; ca. 9.6–8.6 ka) is dominated by *Staurosirella pinnata* (33%), *Cyclotella ocellata* (18%), and other small fragilarioid taxa (60%) (Fig. 3). By ca. 9.0 ka the abundance of *S. pinnata* decreases to 10% and the planktonic species *Cyclotella rossii* (10–30%), *Aulacoseira subarctica* (4–25%) and *Cyclotella ocellata* (5–14%) are more dominant. Some of the small benthic species all show slight increases in abundance at this time, including *Psammothidium levanderi* (9%) and *Achnantheidium minutissimum* (6%), albeit at a low relative abundance.

In Zone 2 (452–352 cm; ca. 8.6–4.4 ka) the planktonic species *C. ocellata*, *A. subarctica*, and *C. rossii* begin to dominate the assemblage (Fig. 3). Collectively these species reach a maximum abundance of 75% between 8.5 and 7.6 ka; a time when small benthic and facultatively planktonic taxa are at their overall lowest Holocene abundances (0–5%). Increases in abundances of *Rossithidium pusillum* and other small fragilarioid taxa occur ca. 7.6 and 6.8 ka, concurrent with a decrease in planktonic taxa (Fig. 3). After ca. 5.0 ka, the abundance of planktonic species gradually decrease, paralleled by increasing abundance of facultatively planktonic taxa.

At the onset of Zone 3 (352–13.25 cm; 4.4 ka–1860 AD) a large increase in the facultatively planktonic taxa is paralleled by declines in planktonic taxa (Fig. 3). Collectively, the small fragilarioid taxa make up ~80% of the assemblages in this zone and several species attain their maximum Holocene abundance, including *S. pinnata* at 4.2 ka (39%) and *Staurosira construens* at 3.8 ka (28%). In contrast, planktonic species decline from a mean abundance of 55% in Zone 2, to 5% in Zone 3. Only *Tabellaria flocculosa* shows relatively little change in abundance from Zone 2, remaining at ~4%. Of the benthic taxa, *Stauroforma exiguiformis* and *R. pusillum* are also present in high abundances throughout Zone 3, with the former attaining a maximum Holocene abundance of 26% at ca. 2.2 ka.

In Zone 4 (13.25–0 cm; ca. 1860–2009 AD) the small fragilarioid taxa continue to dominate the assemblage, comprising ~75% of the total assemblage ca. 1910 AD (Fig. 3). After this time, the abundance of facultatively planktonic taxa steadily decreases as the benthic and planktonic species increase. After ca. 1970 AD, the numbers of *A. subarctica* decreases substantially, such that only a few individual

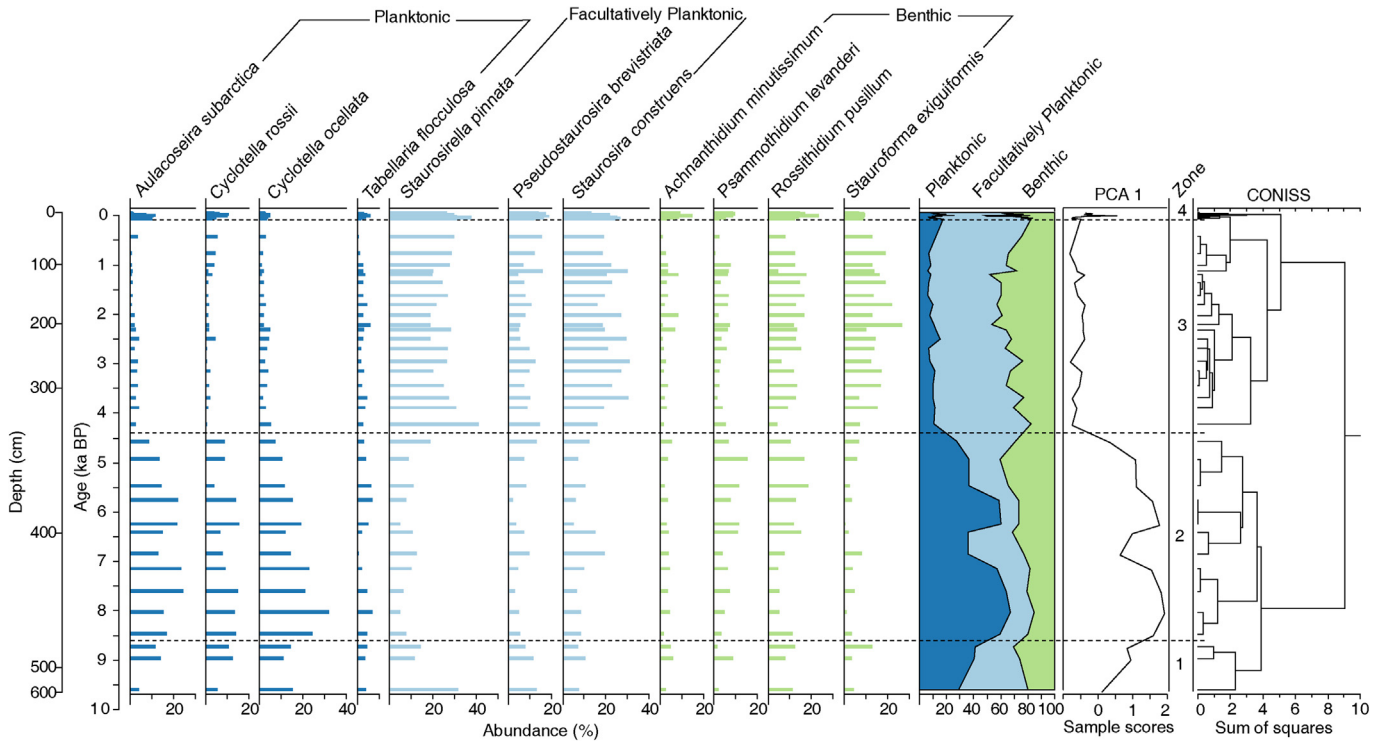


Fig. 3. Heart Lake diatom stratigraphy and Principal Components Analysis (PCA) scores of the 11 dominant diatom species (>5% abundance), grouped by habitat preference. Diatom zone demarcation (dashed lines 1–4) is guided by the CONISS cluster analysis. Variables are plotted on a linear timescale (ka BP) and the depth scale refers to depth below lake floor.

frustules were counted per sample.

Stratigraphic changes in diatom flora are captured in the first two PCA components, which collectively account for 71% of the total assemblage variance (Fig. 4). Additional eigenvectors defined by the PCA (3–5) were not considered given they explain progressively lower proportions of the total variance ($\lambda_3 = 0.108$, $\lambda_4 = 0.059$, $\lambda_5 = 0.038$). PCA 1 represents 57% of total variance and correlates to the planktonic species at the positive extreme, and the facultatively planktonic species at the negative extreme. PCA 2 accounts for 14% of total variance, and correlates to the small fragilarioid taxa (Fig. 4). The Holocene succession of diatom communities in Heart Lake is further illustrated by the time-series of the 54 sample scores on PCA axis 1 (Fig. 3).

4.2. Oxygen isotopes

Holocene $\delta^{18}O_{\text{diatom}}$ values vary between 24.6‰ (1805 AD) and 33.3‰ (7.6 ka) ($\bar{x} = 29.7\text{‰}$, $n = 137$) (Fig. 5) with a range of $\pm 8.7\text{‰}$ that is appreciably greater than the standard deviation of all samples ($\pm 0.19\text{‰}$) and diatom standards ($\pm 0.30\text{‰}$) measured. The base of the Heart Lake sediment core has a $\delta^{18}O_{\text{diatom}}$ value of 29.7‰ at 9.6 ka, and values steadily increase to the maximum Holocene value of 33.3‰ at ca. 7.6 ka (Fig. 5). After 4.9 ka $\delta^{18}O_{\text{diatom}}$ becomes progressively lower until ca. 3.5 ka (27.8‰) where values remain stable at $\sim 29\text{--}30\text{‰}$ until ca. 1.0 ka. After ca. 1.0 ka, $\delta^{18}O_{\text{diatom}}$ exhibits high variability to lower values ca. 1250–1340 AD and 1430–1525 AD, and after 1640 AD there is a shift to overall lower $\delta^{18}O_{\text{diatom}}$ values, including the Holocene minimum $\delta^{18}O_{\text{diatom}}$ value of 24.6‰ at 1805 AD. The $\delta^{18}O_{\text{diatom}}$ values then slightly increase between 1805–1903 AD, before decreasing to the present day (29.8‰) (Fig. 5). Using the sub-division age of 4.2 ka for the mid-late Holocene boundary (Walker et al. 2012), late Holocene $\delta^{18}O_{\text{diatom}}$ is significantly ($p < 0.001$) lower than in the early–mid Holocene.

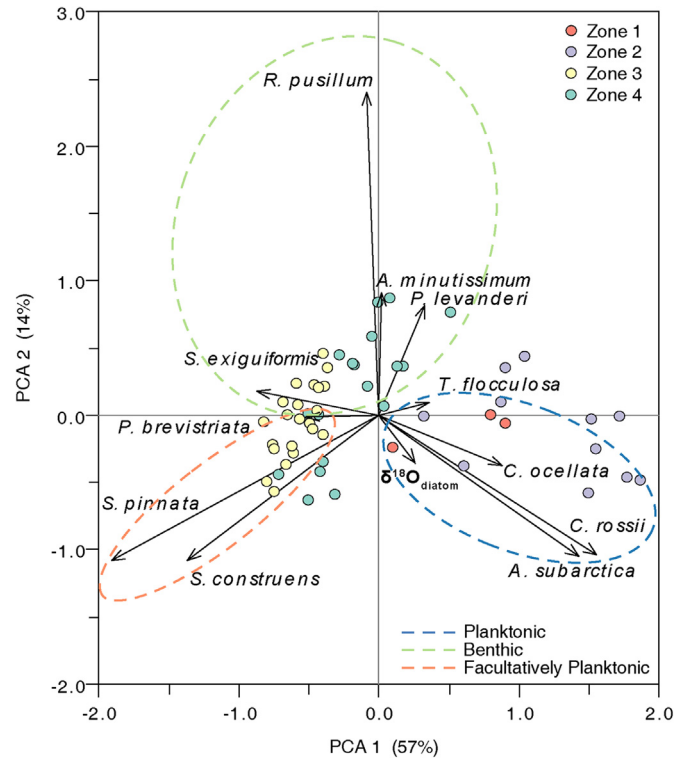


Fig. 4. Loadings of the 11 dominant diatom taxa from Heart Lake and their corresponding PCA scores. Sample scores (circles) are coloured according to their down core diatom assemblage Zone (1–4). Dashed coloured ellipses group diatom species by their habitat preference.

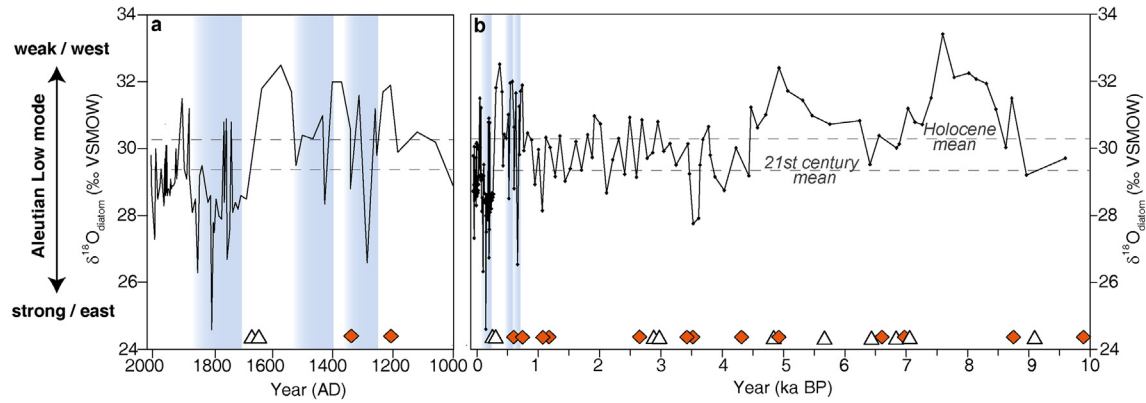


Fig. 5. Time series of Heart Lake $\delta^{18}\text{O}_{\text{diatom}}$ during (a) the past millennium and (b) the Holocene. Horizontal dashed grey lines indicate the Holocene and the 21st century mean $\delta^{18}\text{O}_{\text{diatom}}$ value. Orange diamonds and white triangles indicate previously published radiocarbon ages and tephra beds, respectively (Krawiec et al. 2013). Vertical blue bars correspond to three intervals of Little Ice Age glacier advance in mainland Alaska (Solomina et al. 2015). (For interpretation of the references to colour in this figure legend, the reader is referred to the Web version of this article.)

5. Discussion

5.1. Oxygen isotope paleohydrology and paleoclimatology

Oxygen isotope ratios measured in precipitation ($\delta^{18}\text{O}_p$) at Adak airport (1962–67, 1972–73; $n=60$) indicate mean annual precipitation-weighted $\delta^{18}\text{O}_p$ is -8.8‰ , with small seasonal differences between January (-9.4‰) and July (-8.9‰) (IAEA/WMO, 2017). The correspondence between Heart Lake water $\delta^{18}\text{O}$ and the local and global meteoric water lines confirms that (1) Heart Lake water $\delta^{18}\text{O}$ reflects local precipitation, and (2) evaporative effects influencing precipitation and lake water $\delta^{18}\text{O}$ are minimal with no isotopic enrichment (Fig. 6). Specifically, the two Heart Lake bottom water ($\delta^{18}\text{O}_{\text{water}}$) samples collected in summer 2009 and 2010 ($\bar{x} = -9.5\text{‰}$) are directly comparable, within error, to the long term winter and spring $\delta^{18}\text{O}_p$ values from Adak airport. These

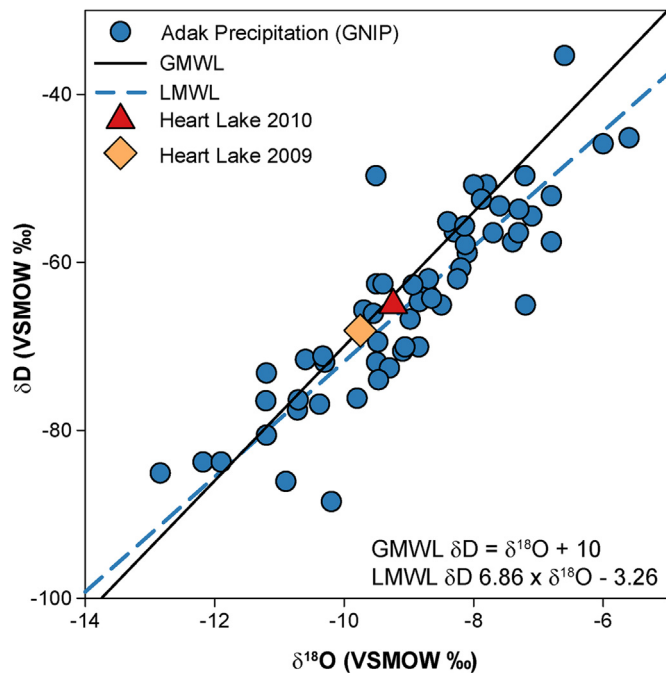


Fig. 6. Heart Lake bottom water $\delta^{18}\text{O}$ (2009 and 2010) on the local meteoric water line (LMWL) and the global meteoric water line (GMWL). LMWL data are derived from Adak monthly composite precipitation samples collected by the Global Network of Isotopes in Precipitation (GNIP) (IAEA/WMO, 2017).

data indicate the lake water budget is dominated by winter and spring precipitation (i.e. snowfall and melt) similar to many lakes and streams across Alaska (Clegg and Hu, 2010; Lachniet et al. 2016; Vachula et al. 2017).

There is no correlation between mean monthly $\delta^{18}\text{O}_p$ and SAT ($r=0.15$, $n=72$) or precipitation amount ($r=0.03$, $n=72$) at Adak airport. Instead, Bailey et al. (2015) found that Adak Island $\delta^{18}\text{O}_p$ values are primarily controlled by the moisture source and trajectory of local precipitating storm systems. Specifically, winters with intensified Aleutian Low circulation are characterized by precipitation with significantly ($p < 0.05$) lower than mean $\delta^{18}\text{O}_p$ values. These variations are explained by systematic shifts in the central foci of the Aleutian Low; when the SLP minimum is near Adak (strong Aleutian Low), polar air masses are drawn south and advect water vapor and precipitation that is relatively depleted in ^{18}O , along with lower-than-average winter temperatures and increased snowfall (Fig. 2b) (Rodionov et al. 2007; Bailey et al. 2015). In contrast, a weakened and westerly displaced Aleutian Low increases the southerly Pacific moisture flux to Adak via an enhanced south-westerly storm track (Fig. 2a) (Rodionov et al. 2007). These systems carry warm ^{18}O -enriched moisture, and bring higher-than-average temperatures and increased precipitation to Adak Island (Bailey et al. 2015).

$\delta^{18}\text{O}_{\text{diatom}}$ is controlled by several environmental parameters which depend on local hydrology, climate, and the seasonality of diatom growth (Barker et al. 2001; Rioual et al. 2001; Jones et al. 2004; Rosqvist et al. 2004; Leng and Barker, 2006; Schiff et al. 2009; Mackay et al. 2011; Meyer et al. 2015; Chaplignin et al. 2016). Previous work by Bailey et al. (2015) showed that the surface core $\delta^{18}\text{O}_{\text{diatom}}$ record from Heart Lake correlates significantly with the winter NPI during the instrumental period (1900–2009 AD) ($r=0.43$, $p < 0.02$, $n=28$). This positive relationship confirms that Heart Lake diatoms precipitate their silica frustule in isotopic equilibrium with the lake water in which they grow (Labeyrie, 1974; Leclerc and Labeyrie, 1987), independent of size or species-related vital effects (Bailey et al. 2014). During the spring thaw, it is evident that winter season precipitation ($\delta^{18}\text{O}_p$) enters Heart Lake coincident with onset of the spring diatom bloom. A limited component of residual summer growth might be expected, but bulk $\delta^{18}\text{O}_{\text{diatom}}$ analysis is weighted toward the main period of diatom growth in spring (Leng et al. 2001; Bailey et al. 2014). Under the assumption that similar climatic controls on $\delta^{18}\text{O}_p$ prevailed before 1900 AD, we use this extended $\delta^{18}\text{O}_{\text{diatom}}$ record as a proxy for atmospheric circulation throughout the Holocene.

5.2. Holocene environmental history of Adak Island

5.2.1. Early-mid Holocene, 9.6–4.4 ka

Adak Island, along with the Aleutian chain, was glaciated during the last glacial maximum, though there are few chronological constraints on the onset and pattern of ice retreat (Coats, 1956; Bradley, 1948; Fraser and Snyder, 1959; Black, 1976). At Heart Lake, percussion coring ceased at a depth of 587 cm without penetrating bedrock or till, indicating the catchment deglaciated prior to 9.6 ka.

From 9.6 to 9.0 ka, the dominance of fragilarioid and other small benthic taxa reflect a temperate oligotrophic shallow lake with an extensive littoral zone. These pioneering taxa dominate polar to subpolar and mountainous tundra lakes (Lotter and Bigler, 2000; Rühland et al. 2003; Hausmann and Pienitz, 2009; Devlin and Finkelstein, 2011) and their presence suggests a relatively short growth season with cool air temperatures (Smol et al. 2005; Rühland et al. 2008; Hausmann and Pienitz, 2009). Cool/dry conditions at this time are further supported by low concentrations of biogenic silica (BSi) and organic matter (OM) in nearby Andrew Lake (Krawiec and Kaufman, 2014) and the dominance of *Salix* and *Empetrum* in northern Adak (Heusser, 1978).

Heart Lake was increasingly colonized by planktonic diatoms between 9.3 and 4.4 ka (Fig. 3). Of these, *A. subarctica* is common across Arctic and subarctic zones, and typically shows pronounced periodicity with the spring maximum in non-stratified lakes (Bradbury et al. 2002; Baier et al. 2004; Rioual et al. 2007; Gibson et al. 2003; Solovieva et al. 2015). It is a heavily silicified species, forming colonies that require turbulence-induced suspension to remain within the photic zone (Rühland et al. 2008; Lotter et al. 2010), and indicates persistent strong seasonal winds, together with associated turbulent water mixing and nutrient upwelling (Wang et al. 2008; Andrén et al. 2015; Solovieva et al. 2015). In contrast, *Cyclotella* species have a competitive advantage over the heavily silicified *A. subarctica* during strong stratification (Andrén et al. 2015) and typically bloom after ice-out in subarctic regions (Rühland et al. 2008; Hoff et al. 2015). In Kamchatka, *Cyclotella* spp. prosper during warmer years (Lepskaya et al. 2010), and are broadly considered warm water indicators due to their recent expansion across Arctic lakes (Smol et al. 2005; Rühland et al. 2008). Collectively, these early-mid Holocene diatom assemblages reveal a phase of overall high lake mixing and turbidity, reduced lake ice cover, and relatively high Si/P ratios (Interlandi et al. 1999; Rühland et al. 2003; Rioual et al. 2007). These changes are further summarized by the Holocene time series of PCA 1 sample scores (Fig. 3).

The isotope composition of Heart Lake water was significantly ($p < 0.001$) higher during the early-mid Holocene compared to the late Holocene (Fig. 5), reflecting the prevalence of southerly storms delivering abundant precipitation with higher $\delta^{18}\text{O}$ values (Bailey et al. 2015). Such warm, southerly winter storms would promote turbulent mixing and limit the development of winter lake ice, thereby extending the open-water growing season and allowing for a spring diatom assemblage dominated by planktonic species (Fig. 3). *Aulacoseira subarctica*, in particular, is abundant in modern lake systems during years with short, warm winters (Gibson et al. 2003; Horn et al. 2011). Elevated pollen percentages of *Cyperaceae* and other wetland species in northern Adak also imply warm/wet conditions at this time (Heusser, 1978) and correspond to higher local lake levels prior to 4.0 ka (Krawiec and Kaufman, 2014). Peak $\delta^{18}\text{O}_{\text{diatom}}$ (33.3‰) suggests maximum Holocene warmth at 7.6 ka, an inference supported by the simultaneous maximum Holocene abundance of the warm water indicator *C. ocellata* (Rühland et al. 2008) (Fig. 3).

The $\delta^{18}\text{O}_{\text{diatom}}$ record correlates positively with the time series of PCA 1 scores ($r = 0.48$, $p < 0.001$) and demonstrates that diatom community structure is indirectly connected to climate over

millennial timescales. It also indicates that diatom species changes are a natural ecological response to climatically-driven shifts in lake water $\delta^{18}\text{O}$, as reflected in the $\delta^{18}\text{O}_{\text{diatom}}$ record, rather than the converse (i.e. changes in diatom species drive $\delta^{18}\text{O}_{\text{diatom}}$ variation).

5.2.2. Mid-late Holocene, 4.4 ka – present

At around 4.4 ka, a major shift in diatom composition occurred with marked changes from a predominantly planktonic assemblage to the dominance of small fragilarioid and benthic taxa (Fig. 3). During this transition the relatively warm, deep, and well-mixed open-water conditions of the early-mid Holocene (9.6–4.4 ka) gave way to a less turbulent, potentially shallower lake. This transition coincides with a shift to lower $\delta^{18}\text{O}_{\text{diatom}}$ values in the late Holocene, reflecting an increase of isotopically depleted water (i.e. snow and/or ice melt) during the spring thaw (Bailey et al., 2015; Streletskiy et al. 2015), and reduced warm, ^{18}O -enriched southerly storms that characterized the early-mid Holocene.

An increase in northerly winds and lower temperatures during the late Holocene would have enhanced formation of winter lake ice, which in turn was insulated and prolonged by increased winter snowfall (Mock et al. 1998). Persistence of lake ice into the spring shortens the aquatic growth season and restricts light penetration into the water column during the spring bloom, thereby precluding the growth and development of planktonic communities requiring an ice-free lake for photosynthesis and a turbulent, well-mixed water column. Instead, the mid-late Holocene flora at Heart Lake is dominated by fragilarioid species known to colonise benthic and periphytic habitats under lake ice cover (Lotter and Bigler, 2000; Douglas and Smol, 2010; Biskaborn et al. 2016). These benthic communities would have further benefitted from the absence of competition for nutrients from planktonic diatoms, which do not thrive under ice (Lepskaya et al. 2010; Roberts et al. 2015). A reduction in turbulent wind-driven lake mixing at this time may have also been responsible for increased benthic production and a simultaneous expansion of the littoral zone and benthic habitat (Bradbury et al., 2002). Increased winter precipitation and subsequent spring snow melt would account for the sedimentation increase at 3.8 ka from 0.2 to 0.8 mm/yr (Krawiec and Kaufman, 2014). This turbidity would have further reduced light penetration into the benthic zone, thereby promoting fragilarioid taxa which thrive under limited light and generally turbid conditions (Lotter and Bigler, 2000; Douglas and Smol, 2010).

The simultaneous changes in diatom species assemblages and $\delta^{18}\text{O}_{\text{diatom}}$ values ca. 4.4 ka reflect numerous factors affecting vertical mixing patterns, availability of resources (e.g. light, nutrients), and thereby the algal production and composition of Heart Lake. These pronounced changes broadly coincided with other paleoenvironmental changes on Adak Island centred ca. 4.4 ka. For example the BSi and inferred chlorophyll-*a* record from nearby Andrew Lake also indicates increased aridity after 4.0 ka (Krawiec and Kaufman, 2014), while reconstructed plant assemblages show a reduction in *Cyperaceae* after ca. 4.5 ka as cooler/drier conditions prevailed over Adak Island (Heusser, 1978).

Between 950 AD and 1200 AD, higher $\delta^{18}\text{O}_{\text{diatom}}$ indicates a transition to overall warmer and wetter conditions on Adak (Fig. 5). A decrease in *Empetrum* vegetation across northern Adak also indicates increased moisture (Heusser, 1978), while Krawiec and Kaufman (2014) interpret sustained low BSi and chlorophyll-*a* content from Andrew Lake as the stormiest interval on record. Our $\delta^{18}\text{O}_{\text{diatom}}$ values exhibit high variability between 950 and 1900 AD, implying the local climate was also wetter and more variable since 950 AD. These conditions would account for the continued dominance of fragilarioid taxa over this period with unstable lake conditions (Smol et al. 2005; Rühland et al. 2008; Hausmann and Pienitz, 2009). Additionally, a peak in sedimentation ca. 1.0 ka,

attributed to increased storminess (Krawiec and Kaufman, 2014), rendered conditions unfavourable for planktonic diatom species due to increased sediment suspension and reduced light penetration. Unlike numerous diatom assemblage records across the sub-arctic and Arctic, in Heart Lake there is no major shift toward those taxa favouring longer growing seasons under warming climatic conditions (e.g. *Cyclotella*) (Smol et al. 2005). Conversely, benthic assemblages show an increase after ca. 1860 AD (Fig. 3), reflecting an overall strengthening of Aleutian Low circulation since 1900 AD (Trenberth and Hurrell, 1994) and increasingly unstable environmental conditions on Adak Island over the past century. These findings are consistent with observations in North America and Greenland that suggest shifts in *Cyclotella* abundances are more closely related to lake mixing, water clarity and resource availability, rather than direct temperature effects (Saros and Anderson, 2015).

5.3. Regional paleoenvironmental context

Our $\delta^{18}\text{O}_{\text{diatom}}$ reconstruction reveals distinct shifts in the prevailing trajectory of storm systems delivering moisture to Adak Island. The primary trends suggest a relatively weak and westerly positioned Aleutian Low during the early-mid Holocene (9.7–4.5 ka), with a strengthening eastward shift after ca. 4.5 ka (Fig. 5). Based on 21st century observations, typical climatic responses to a weakened Aleutian Low are: (1) a weakening of Pacific mid-latitude storm tracks; (2) increased meridional flow to the central-western Bering Sea; and (3) reduced winter sea surface heat loss in the central-western Bering Sea and enhanced heat loss from the Okhotsk Sea (Mock et al. 1998; Rodionov et al. 2007). Under this synoptic regime the following conditions would be anticipated in regional paleoclimate records: (1) a reduction in winter storms and precipitation in the Gulf of Alaska region; (2) positive precipitation and temperature anomalies in the central-western Aleutian Islands; and (3) SST warming and reduced winter sea ice extent in the central-western Bering Sea and contrary conditions in the Okhotsk Sea.

In support of this synoptic-scale picture, vegetation and lake-level reconstructions provide independent evidence for considerably drier winter conditions in eastern Beringia during the early-mid Holocene (Anderson et al. 2005; RS Anderson et al., 2006; Zander et al. 2013). For example, numerous lakes in southern Alaska and the Yukon record lower-than-present water levels during the early Holocene until ca. 8 ka (Kaufman et al. 2016), reflecting a combination of higher summer temperatures and lower winter precipitation. Furthermore, an inferred decrease in frequency and intensity of winter storms steered into the Gulf of Alaska accounts for marked episodes of glacial retreat at this time (Solomina et al. 2015), driven by reduced winter snowfall/accumulation and negative net mass balance.

The SST patterns associated with a weakened wintertime Aleutian Low are also evident during the early-mid Holocene. Relatively warm early Holocene SSTs are documented from the western Bering Sea (Max et al. 2012), reflecting a persistently negative phase of the PDO during the early-mid Holocene and an increase in Pacific storms tracking into the region (Rodionov et al. 2007). In the Okhotsk Sea, alkenone-derived SST estimates correspond well with Heart Lake $\delta^{18}\text{O}_{\text{diatom}}$ between ca. 9.6–5.0 ka (Fig. 7), whereby higher $\delta^{18}\text{O}_{\text{diatom}}$ and an inferred weak Aleutian Low corresponds to lower early-mid Holocene SSTs (Max et al. 2012). This relationship conforms to modern northerly geostrophic wind anomalies during a weakened and westward displaced Aleutian Low that cool and enhance polynya growth in the Okhotsk Sea (Itaki and Ikahara, 2004; Harada et al. 2014). Specifically, warm (cold) winter SSTs in the Bering Sea (Okhotsk

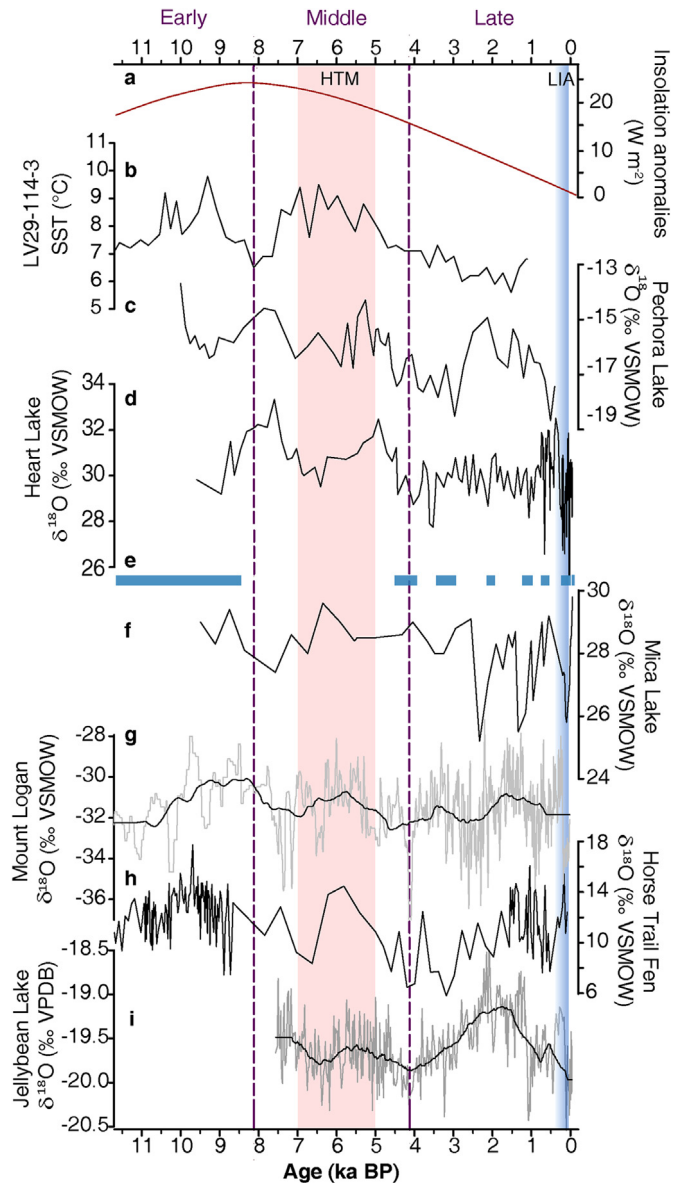


Fig. 7. Holocene time series of (a) summer (JJA) insolation at 65°N (Berger and Loutre, 1991), (b) alkenone SSTs from LV29-114-3 in the Okhotsk Sea (Max et al. 2012), (c) Pechora Lake $\delta^{18}\text{O}$ (Hammarlund et al. 2015), (d) Heart Lake $\delta^{18}\text{O}_{\text{diatom}}$ (this record), (e) intervals of expanded mountain glaciers in eastern Beringia (Solomina et al. 2015), (f) Mica Lake $\delta^{18}\text{O}$ (Schiff et al. 2009), (g) Mount Logan ice $\delta^{18}\text{O}$ (Fisher et al. 2008), (h) Horse Trail Fen $\delta^{18}\text{O}$ (Jones et al. 2014), and (i) Jellybean Lake $\delta^{18}\text{O}$ (Anderson et al. 2005). Black lines in (g) and (i) represent 40-yr smoothed intervals. Vertical red shading indicates the eastern Beringia mid-Holocene Thermal Maximum (Kaufman et al. 2016), blue shading indicates the Little Ice Age (LIA) (Solomina et al. 2015). (For interpretation of the references to colour in this figure legend, the reader is referred to the Web version of this article.)

Sea) presently occur when the Aleutian Low is shifted west and the Siberian High dominates over central western Siberia (Rodionov et al. 2007). These anti-correlated trends also manifest in sea-ice anomalies on weekly to monthly time-scales during the 21st century (Cavalieri and Parkinson, 1987) and are linked to the east–west migration of the Siberian High and Aleutian Low.

We find independent support for the Holocene migration of the Siberian High from the Pechora Lake $\delta^{18}\text{O}$ record in northern Kamchatka (Hammarlund et al. 2015) (Fig. 7). A north-eastward shift of the Siberian High, concurrent with a strong and eastward shifted Aleutian Low, is linked to periods of increased winter snow

contributions to Pechora Lake and overall lower $\delta^{18}\text{O}$ values (Hammarlund et al. 2015). The coherency of abrupt and persistent change between the Heart and Pechora Lake $\delta^{18}\text{O}$ records between 9.6 and 3.5 ka provides convincing evidence that the Aleutian Low–Siberian High system prevailed throughout the early-mid Holocene (Fig. 7). Moreover, we propose that the synchronous west-east migration of these systems may have been partially responsible for the non-linear and heterogeneous climatic patterns reconstructed across east and west Beringia at this time (Brooks et al. 2015; Kaufman et al. 2016).

Maximum values of $\delta^{18}\text{O}_{\text{diatom}}$ in Heart Lake at 7.6 ka broadly coincide with the northern high-latitude (65 °N) summer insolation maxima ca. 8.0 ka (Fig. 7) (Berger and Loutre, 1991). Significantly ($p < 0.001$) higher $\delta^{18}\text{O}_{\text{diatom}}$ in Heart Lake – relative to both the modern (1900 AD–present) and long-term (9.6 ka–present) mean $\delta^{18}\text{O}_{\text{diatom}}$ – implies a HTM in the central Aleutian Islands at 7.6 ka characterized by persistently weak Aleutian Low circulation, and coincident with maximum abundances of warm water indicator species (Smol et al. 2005) (Fig. 3). Similarly, a Holocene SST maximum is evident ca. 7.5 ka in both the northwest Pacific (Minoshima et al. 2007) and the subarctic North Pacific (Harada et al. 2014), and from GCMs which indicate maximum SATs and SSTs in the Bering Sea and Aleutian Islands ca. 7.0–8.0 ka (Renssen et al. 2012). In southern Kamchatka, the majority of paleoenvironmental records demonstrate a HTM ca. 7.0–5.3 ka (Brooks et al. 2015), consistent with warm temperatures across eastern Beringia (Kaufman et al. 2016). These results contrast with previous paleoclimate studies from Alaska and the northwest Pacific that identify an earlier HTM at ca. 11.3–9.1 ka (Kaufman et al. 2004; Max et al. 2012). Such uncertainty in these early Holocene warming patterns is highlighted by Zhang et al. (2017) who found large discrepancies between modelled and reconstructed Holocene temperatures across Alaska. Hence, it is difficult to fully constrain the timing of the HTM in the central Aleutian Islands, particularly given that our record does not extend the full Holocene epoch coupled with a paucity of local alternative studies.

Simultaneous shifts in diatom flora and $\delta^{18}\text{O}_{\text{diatom}}$ after the HTM at ca. 4.5 ka indicate multiple and inter-related environmental changes that impacted Heart Lake. These pronounced changes coincide with local proxy inferences demonstrating increased aridity under a prevailing northerly circulation pattern (Heusser, 1978; Corbett et al. 2010; Krawiec and Kaufman, 2014). This mid-Holocene perturbation coincides with a return to cooler conditions, increased winter precipitation and extensive glacial advance in Kamchatka (Nazarova et al. 2013; Barr and Solomina, 2014; Meyer et al. 2015). Widespread cooling is also evident in eastern Beringia during the late Holocene (Kaufman et al. 2016), and mountain glaciers across Alaska advanced between ca. 4.5 and 3.0 ka (Solomina et al. 2015), in phase with those in Kamchatka and demarking onset of the Neoglacial across Beringia (Savoskul, 1999; Barr and Solomina, 2014). Though temperature is proposed as the principal control on regional glacier mass balance through the Holocene (Solomina et al. 2015), the observed glacial maxima in Alaska are asynchronous with the timing of pronounced cold intervals (Kaufman et al. 2016). Instead, our data suggest the transition to intensified Aleutian Low circulation after 4.5 ka, coincident with declining summer insolation (Berger and Loutre, 1991), drove widespread Neoglacial advance through the combined effect of increased winter snowfall under a generally cooler regime, yielding a marked regional positive mass balance perturbation. In particular, we note during the past millennium three intervals of lower $\delta^{18}\text{O}_{\text{diatom}}$ values between 1275–1350 AD, 1400–1550 AD, and 1700–1850 AD coincide with three well-documented episodes of Little Ice Age (LIA) glacier advance on mainland Alaska (Figs. 5 and 7) (Calkin et al. 2001; Solomina et al. 2015). Furthermore, the

$\delta^{18}\text{O}_{\text{diatom}}$ minimum at 1805 AD (+24.6‰) marks the culmination of regional LIA glacial advance (Barclay et al. 2009; Calkin et al. 2001; Wiles et al. 2004; Solomina et al. 2015) (Figs. 5 and 7).

5.4. Coherency of paleoisotope trends

Several paleoisotope records from Alaska have also been interpreted in terms of synoptic-scale changes in atmospheric circulation and inter-comparison with Heart Lake $\delta^{18}\text{O}_{\text{diatom}}$ yields many commonalities and insights (Anderson et al. 2005; Fisher et al. 2004, 2008; Schiff et al. 2009; Jones et al. 2014; Hammarlund et al. 2015) (Fig. 7). For instance, a strong inverse relationship ca. 9.5–4.0 ka is apparent with millennial scale $\delta^{18}\text{O}_{\text{diatom}}$ variations at Mica Lake, in Prince William Sound (Schiff et al. 2009) (Fig. 7). Lower Mica Lake $\delta^{18}\text{O}_{\text{diatom}}$ values indicate precipitation delivered by zonal flow under a weak Aleutian Low, whereby precipitating systems are subject to increased rainout as they pass over the Kenai Peninsula and coastal mountain ranges. Conversely, increased meridional flow during a strong Aleutian Low delivers locally sourced moisture from nearby Gulf of Alaska, thereby reducing distillation and isotope depletion in precipitation, thus yielding higher Mica Lake $\delta^{18}\text{O}_{\text{diatom}}$ values (Schiff et al. 2009). The reciprocal relationship between precipitation-inferred $\delta^{18}\text{O}$ values at Heart and Mica Lakes between ca. 9.5–4.0 ka conforms to modelling and empirical analyses of spatial patterns of $\delta^{18}\text{O}_p$ (Berkelhammer et al. 2012; Bailey et al. 2015). The Horse Trail Fen record from the Kenai lowlands is also comparable to Heart Lake from ca. 8.0 ka and demonstrates overall higher $\delta^{18}\text{O}$ values during the early Holocene and reflecting generally weak Aleutian Low circulation (Jones et al. 2014). The only other full Holocene paleoisotope record from eastern Beringia is from the Mount Logan ice core (Fisher et al. 2008), which exhibits strong correspondence with the Jellybean (Anderson et al. 2005) and Heart Lake $\delta^{18}\text{O}$ records during the early-mid Holocene (Fig. 7).

Secondary, but notable departures between paleoisotope records are evident during the late Holocene (Fig. 7), some of which can be reconciled by considering the detailed, non-linear complexity of atmospheric circulation. For instance between ca. 3.0–1.0 ka Heart Lake $\delta^{18}\text{O}_{\text{diatom}}$ does not exhibit marked excursions to the higher $\delta^{18}\text{O}$ values documented in Mt. Logan, Jellybean and Pechora Lakes, interpreted as an interval of pronounced weak Aleutian Low circulation (Anderson et al. 2005; Fisher et al. 2008; Hammarlund et al. 2015). At Heart Lake, this period is characterized by $\delta^{18}\text{O}_{\text{diatom}}$ values closer to the Holocene mean (Fig. 7). These differences could reflect prevailing atmospheric patterns characterized by a more southerly displaced western centre of low pressure in the northwest Pacific, which typically results in a higher density of storms being steered into the Gulf of Alaska and eastern Kamchatka Peninsula (Mock et al. 1998; Rodionov et al. 2007). Under such conditions, precipitation at Mt. Logan, Jellybean and Pechora Lakes would be relatively ^{18}O -enriched (Berkelhammer et al. 2012), whereas Heart Lake would fail to exhibit higher $\delta^{18}\text{O}_{\text{diatom}}$ values since these storm systems would track south of the Aleutian Islands (Rodionov et al. 2007).

6. Conclusions

The new datasets and analysis presented here extend modern observations across Alaska and Siberia back through the Holocene to bridge a critical gap in the regional network of proxy-climate records (Sundqvist et al. 2014; Brooks et al. 2015; Kaufman et al. 2016). Although GCMs typically emphasise insolation as the key driver of Holocene temperature change in Alaska (Renssen et al. 2009), we demonstrate a more complex relationship and emphasise the role of moisture availability and transport within the

land–atmosphere–ocean system.

The Aleutian Islands straddle a critical zone of cyclogenesis that influences regional temperature and precipitation patterns, including the heat and moisture flux between the extratropical Pacific and Arctic; hence, the variable modes of atmospheric circulation we identify have a wide reaching global influence through atmospheric–oceanic teleconnections. Our empirically-derived understanding of the drivers and magnitude of these past changes provide a means to contextualise contemporary climate trends, along with their potential future trajectory and impact, across Alaska and the wider North Pacific. Specifically, we demonstrate that Holocene shifts in Aleutian Low circulation directly impacted the net mass balance of south-central Alaska's glaciers and ice fields through temperature and precipitation variability (Solomina et al. 2015). Given that Alaska is currently experiencing a period of intensified Aleutian Low circulation, which should be favorable for glacier *growth*, the widespread and well documented 21st century retreat of glaciers and ice cover (Larsen et al. 2015) would now appear to be unprecedented within the context of long-term Holocene environmental change.

Author contributions

D.S.K was PI, led the fieldwork and retrieved the sediment cores. D.S.K., H.L.B, H.J.S., A.C.G.H. and M.J.L developed the study concept. H.L.B conducted the research, sample preparation, SEM, diatom and statistical analyses, interpreted the results, produced the figures, and wrote the original manuscript. D.S.K. and A.L.H. critically revised the original manuscript, and together with H.M. and J.M.W. provided technical advice and comments. H.J.S performed the FTIR and diatom isotope measurements. M.J.L. supervised the diatom isotope measurements and undertook the isotope corrections. H.J.S., A.C.G.H., M.J.L., H.M. and J.M.W provided minor editorial revisions. All authors approved the final manuscript.

The authors declare no competing financial interests.

Data availability

Key datasets for this study are available in [Supplementary Table 1](#). All data produced by this study are available online at the World Data Centre for Paleoclimatology (WDC Paleo) (<https://www.ncdc.noaa.gov/data-access/paleoclimatology-data>) and in the NERC National Geoscience Data Centre (NGDC) (<http://www.bgs.ac.uk/services/ngdc/>).

Acknowledgements

This research was funded by NSF award EAR 0823522, NERC grants IP/1202/1110 and IP/1460/0514, and a NERC CASE award to H.L.B. (NE/I528350/1). The research was further supported by a Lloyds of London Fulbright Fellowship award to H.L.B. during the preparation of this manuscript. We thank Yarrow Axford, Anne Krawiec, Caleb Schiff, and David Vaillencourt for their field assistance. The US Fish and Wildlife Service, Alaska Maritime Natural Wildlife Refuge and CPS Polar services provided logistical support and access for fieldwork on Adak Island.

Appendix A. Supplementary data

Supplementary data related to this article can be found at <https://doi.org/10.1016/j.quascirev.2018.06.027>.

References

Anderson, L., Abbot, M.B., Finney, B.P., Burns, S.J., 2005. Regional atmospheric

- circulation change in the North Pacific during the Holocene inferred from lacustrine carbonate oxygen isotopes, Yukon Territory, Canada. *Quat. Res.* 64, 21–35. <https://doi.org/10.1016/j.yqres.2005.03.005>.
- Anderson, R.S., Hallett, D.J., Berg, E., Jass, R.B., Toney, J.L., De Fontaine, C.S., DeVolder, A., 2006. Holocene development of boreal forests and fire regimes on the Kenai Lowlands of Alaska. *Holocene* 16 (6), 791–803. <https://doi.org/10.1191/0959683606hol966rp>.
- Anderson, L., Berkelhammer, M., Barron, J.A., Steinman, B.A., Finney, B.P., Abbott, M.B., 2016. Lake oxygen isotopes as recorders of North American Rocky Mountain hydroclimate: Holocene patterns and variability at multi-decadal to millennial timescales. *Global Planet. Change* 137, 131–148. <https://doi.org/10.1016/j.gloplacha.2015.12.021>.
- Andrén, E., Klimaschewski, A., Self, A.E., Amour, N.S., Andreev, A.A., Bennett, K.D., Conley, D.J., Edwards, T.W.D., Solovieva, N., Hammarlund, D., 2015. Holocene climate and environmental change in north-eastern Kamchatka (Russian Far East), inferred from a multi-proxy study of lake sediments. *Global Planet. Change* 134, 41–54. <https://doi.org/10.1016/j.gloplacha.2015.02.013>.
- Baier, J., Lücke, A., Negendank, J.F., Schleser, G.H., Zolitschka, B., 2004. Diatom and geochemical evidence of mid-to late Holocene climatic changes at Lake Holzmaar, West-Eifel (Germany). *Quat. Int.* 113 (1), 81–96. [https://doi.org/10.1016/S1040-6182\(03\)00081-8](https://doi.org/10.1016/S1040-6182(03)00081-8).
- Bailey, H.L., Henderson, A.C.G., Sloane, H.J., Snelling, A., Leng, M.J., Kaufman, D.S., 2014. The effects of species on lacustrine $\delta^{18}\text{O}_{\text{diatom}}$ and its implications for environmental reconstructions. *J. Quat. Sci.* 29, 393–400. <https://doi.org/10.1002/jqs.2711>.
- Bailey, H.L., Kaufman, D.S., Henderson, A.C.G., Leng, M.J., 2015. Synoptic scale controls on the $\delta^{18}\text{O}$ in precipitation across Beringia. *Geophys. Res. Lett.* 42, 4608–4616. <https://doi.org/10.1002/2015GL063983>.
- Barclay, D.J., Wiles, G.C., Calkin, P.E., 2009. Holocene glacier fluctuations in Alaska. *Quat. Sci. Rev.* 28, 2034–2048. <https://doi.org/10.1016/j.quascirev.2009.01.016>.
- Barker, P.A., Street-Perrott, F.A., Leng, M.J., Greenwood, P.B., Swain, D.L., Perrott, R.A., Telford, J., Ficken, K.J., 2001. A 14 ka oxygen isotope record from diatom silica in two alpine tarns on Mt. Kenya. *Science* 292, 2307–2310. <https://doi.org/10.1126/science.1059612>.
- Barr, I.D., Solomina, O., 2014. Pleistocene and Holocene glacier fluctuations upon the Kamchatka Peninsula. *Glob. Planet. Change* 113, 110–120. <https://doi.org/10.1016/j.gloplacha.2013.08.005>.
- Berger, A., Loutre, M.F., 1991. Insolation values for the climate of the last 10 million years. *Quat. Sci. Rev.* 10, 297–317. [https://doi.org/10.1016/0277-3791\(91\)90033-Q](https://doi.org/10.1016/0277-3791(91)90033-Q).
- Berkelhammer, M., Stott, L., Yoshimura, K., Johnson, K., Sinha, A., 2012. Synoptic and mesoscale controls on the isotopic composition of precipitation in the western United States. *Clim. Dynam.* 38 (3–4), 433–454. <https://doi.org/10.1007/s00382-011-1262-3>.
- Biskaborn, B.K., Subetto, D.A., Savelieva, L.A., Vakhrameeva, P.S., Hansche, A., Herzschuh, U., Klemm, J., Heinecke, L., Pestryakova, L.A., Meyer, H., Kuhn, G., 2016. Late Quaternary vegetation and lake system dynamics in north-eastern Siberia: implications for seasonal climate variability. *Quat. Sci. Rev.* 147, 406–421. <https://doi.org/10.1016/j.quascirev.2015.08.014>.
- Black, R.F., 1976. Late quaternary glacial events, Aleutian islands, Alaska. In: Easterbrook, D.D., Sibrava, V. (Eds.), *Quaternary Glaciations in the Northern Hemisphere*. IUGS/UNESCO International Geological Correlations Program, Project 73-1-24. International Union of Quaternary Research, Bellingham, pp. 285–301.
- Bradbury, P., Cumming, B., Laird, K., 2002. A 1500-year record of climatic and environmental change in Elk Lake, Minnesota III: measures of past primary productivity. *J. Paleolimnol.* 27 (3), 321–340. <https://doi.org/10.1023/A:1016035313101>.
- Bradley, C.C., 1948. Geologic notes on Adak island and the Aleutian chain, Alaska. *Am. J. Sci.* 246 (4), 214–240. <https://doi.org/10.2475/ajs.246.4.214>.
- Brooks, S.J., Diekmann, B., Jones, V.J., Hammarlund, D., 2015. Holocene environmental change in Kamchatka: a synopsis. *Global Planet. Change* 134, 166–174. <https://doi.org/10.1016/j.gloplacha.2015.09.004>.
- Calkin, P.E., Wiles, G.C., Barclay, D.J., 2001. Holocene coastal glaciation of Alaska. *Quat. Sci. Rev.* 20, 449–461. [https://doi.org/10.1016/S0277-3791\(00\)00105-0](https://doi.org/10.1016/S0277-3791(00)00105-0).
- Camburn, K.E., Charles, D.F., 2000. *Diatoms of Low-alkalinity Lakes in the North-eastern United States*. ANSP Special Publication 18. Academy of Natural Sciences of Philadelphia, Philadelphia.
- Cavaliere, D.J., Parkinson, C.L., 1987. On the relationship between atmospheric circulation and the fluctuations in the sea ice extents of the Bering and Okhotsk Seas. *J. Geophys. Res.* 92, 7141–7162. <https://doi.org/10.1029/JC092iC07p07141>.
- Chaplin, B., Narancic, B., Meyer, H., Pienitz, R., 2016. Paleo-environmental gateways in the eastern Canadian arctic—Recent isotope hydrology and diatom oxygen isotopes from Nettilling Lake, Baffin Island, Canada. *Quat. Sci. Rev.* 147, 379–390. <https://doi.org/10.1016/j.quascirev.2016.03.028>.
- Clayton, R.N., Mayeda, T.K., 1963. The use of bromine pentafluoride in the extraction of oxygen from oxide and silicates for isotopic analysis. *Geochem. Cosmochim. Acta* 27, 43–52. [https://doi.org/10.1016/0016-7037\(63\)90071-1](https://doi.org/10.1016/0016-7037(63)90071-1).
- Clegg, B.F., Hu, F.S., 2010. An oxygen-isotope record of Holocene climate change in south-central Brooks Range, Alaska. *Quat. Sci. Rev.* 29, 928–939. <https://doi.org/10.1016/j.quascirev.2009.12.009>.
- Coats, R.R., 1956. *Reconnaissance Geology of Some Western Aleutian Islands*. US Geological Survey Bulletin 1028-E, Government Printing Office, Alaska.
- Corbett, D., West, D., Lefevre, C., 2010. *The People at the End of the World: the Western Aleutian Project and the Archeology of Shemya Island, Alaska*. Anthropological Association Monograph Series VIII.

- Devlin, J.E., Finkelstein, S.A., 2011. Local physiographic controls on the responses of Arctic lakes to climate warming in Sirmilik National Park, Nunavut, Canada. *J. Paleolimnol.* 45 (1), 23–39. <https://doi.org/10.1007/s10933-010-9477-6>.
- Douglas, M.S.V., Smol, J.P., 2010. Freshwater diatoms as indicators of environmental change in the High Arctic. In: Smol, J.P., Stoermer, E.F. (Eds.), *The Diatoms: Application for the Environmental and Earth Sciences*. Cambridge University Press, Cambridge, pp. 249–266.
- Fisher, D.A., Wake, C., Kreutz, K., Yalcin, K., Steig, E., Mayewski, P., Anderson, L., Zheng, J., Rupper, S., Zdanowicz, C., Demuth, M., Waszkiewicz, M., Dahl-Jensen, D., Goto-Azuma, K., Bourgeois, J.B., Koerner, R.M., Sekerka, J., Osterberg, E., Abbott, M.B., Finney, B.P., Burn, S.J., 2004. Stable isotope records from Mount Logan, Eclipse ice cores and nearby Jellybean Lake. Water cycle of the North Pacific over 2000 years and over five vertical kilometres: sudden shifts and tropical connections. *Géogr. Phys. Quaternaire* 58 (2–3), 337–352. <https://doi.org/10.7202/013147ar>.
- Fisher, D., Osterberg, E., Dyke, A., Dahl-Jensen, D., Demuth, M., Zdanowicz, C., Bourgeois, J., Koerner, R.M., Mayewski, P., Wake, C., Kreutz, K., Steig, E., Zheng, J., Yalcin, K., Goto-Azuma, K., Luckman, B., Rupper, S., 2008. The Mt Logan holocene-late wisconsinan isotope record: tropical Pacific–Yukon connections. *Holocene* 18, 667–677. <https://doi.org/10.1177/0959683608092236>.
- Fraser, G.D., Snyder, G.L., 1959. *Geology of Southern Adak Island and Kagalska Island*. Alaska, US Geological Survey Bulletin 1028, pp. 371–408.
- Gibson, C.E., Anderson, N.J., Haworth, E.Y., 2003. *Aulacoseira subarctica*: taxonomy, physiology, ecology and palaeoecology. *Eur. J. Phycol.* 38, 83–101. <https://doi.org/10.1080/0967026031000094102>.
- Grimm, E.C., 1987. CONISS - a Fortran-77 program for stratigraphically constrained cluster-analysis by the method of incremental sum of squares. *Comput. Geosci.* 13, 13–35.
- Grimm, E.C., 2015. TILIA Software. Version 2.0.41. <https://www.tiliasoft.com/download/>.
- Hammarlund, D., Klimaschewski, A., St Amour, N.A., Andrén, E., Self, A.E., Solovieva, N., Andreev, A.A., Barnekowa, L., Edwards, T.W.D., 2015. Late Holocene expansion of Siberian dwarf pine (*Pinus pumila*) in Kamchatka in response to increased snow cover as inferred from lacustrine oxygen-isotope records. *Global Planet. Change* 134, 91–100. <https://doi.org/10.1016/j.gloplacha.2015.04.004>.
- Harada, N., Katsuki, K., Nakagawa, M., Matsumoto, A., Seki, O., Addison, J.A., Finney, B.P., Sato, M., 2014. Holocene sea surface temperature and sea ice extent in the Okhotsk and Bering Seas. *Prog. Oceanogr.* 126, 242–253. <https://doi.org/10.1016/j.pcean.2014.04.017>.
- Hausmann, S., Pienitz, R., 2009. Seasonal water chemistry and diatom changes in six boreal lakes of the Laurentian Mountains (Québec, Canada): impacts of climate and timber harvesting. *Hydrobiologia* 635 (1), 1–14. <https://doi.org/10.1007/s10750-009-9855-0>.
- Heusser, C.J., 1978. Post-glacial vegetation on Adak island, Aleutian islands, Alaska. *Bull. Torrey Bot. Club* 105, 18–23. <https://doi.org/10.2307/2484259>.
- Hoff, U., Biskaborn, B.K., Dirksen, V.G., Dirksen, O., Kuhn, G., Meyer, H., Nazarova, L., Roth, A., Diekmann, B., 2015. Holocene environment of central Kamchatka, Russia: implications from a multi-proxy record of two-Yurts lake. *Global Planet. Change* 134, 101–117. <https://doi.org/10.1016/j.gloplacha.2015.07.011>.
- Horn, H., Paul, L., Horn, W., Petzoldt, T., 2011. Long-term trends in the diatom composition of the spring bloom of a German reservoir: is *Aulacoseira subarctica* favoured by warm winters? *Freshw. Biol.* 56 (12), 2483–2499. <https://doi.org/10.1111/j.1365-2427.2011.02674.x>.
- IAEA/WMO, 2017. Global Network of Isotopes in Precipitation. The GNIP Database. Accessible at: <http://www.iaea.org/water>.
- Interlandi, S.J., Kilham, S.S., Theriot, E.C., 1999. Responses of phytoplankton to varied resource availability in large lakes of the Greater Yellowstone Ecosystem. *Limnol. Oceanogr.* 44 (3), 668–682. <https://doi.org/10.4319/lo.1999.44.3.0668>.
- Itaki, T., Ikehara, K., 2004. Middle to late Holocene changes of the Okhotsk Sea Intermediate Water and their relation to atmospheric circulation. *Geophys. Res. Lett.* 31, L24309. <https://doi.org/10.1029/2004GL021384>.
- Jones, V.J., Leng, M.J., Solovieva, N., Sloane, H.J., Tarasov, P., 2004. Holocene climate of the Kola Peninsula; evidence from the oxygen isotope record of diatom silica. *Quat. Sci. Rev.* 23 (7–8), 833–839. <https://doi.org/10.1016/j.quascirev.2003.06.014>.
- Jones, M.C., Wooller, M., Peteet, D.M., 2014. A deglacial and Holocene record of climate variability in south-central Alaska from stable oxygen isotopes and plant macrofossils in peat. *Quat. Sci. Rev.* 87, 1–11. <https://doi.org/10.1016/j.quascirev.2013.12.025>.
- Juggins, S., 2014. *C2 Data Analysis. Version 1.7.6*. University of Newcastle, Newcastle.
- Kalnay, E., et al., 1996. The NCEP/NCAR 40-year reanalysis project. *Bull. Am. Meteorol. Soc.* 77, 437–471.
- Kaufman, D.S., Ager, T.A., Anderson, N.J., Anderson, P.M., Andrews, J.T., Bartelein, P.J., Burbaker, L.B., Coats, L.L., Cwynar, L.C., Duval, M.L., Dyke, A.S., Edwards, M.E., Eiser, W.R., Gajewski, K., Geisodottir, A., Hu, F.S., Jennings, A.E., Kaplan, M.R., Kewin, M.W., Lozhkin, A.V., MacDonald, G.M., Miller, G.H., Mock, C.J., Oswald, W.W., Otto-Blisner, B.L., Porcinhu, D.F., Rühland, K., Smol, J.P., Steig, E.J., Wolfe, B.B., 2004. Holocene thermal maximum in the western Arctic (0–180° W). *Quat. Sci. Rev.* 23, 529–560. <https://doi.org/10.1016/j.quascirev.2003.09.007>.
- Kaufman, D.S., Axford, Y.L., Henderson, A.C.G., McKay, N.P., Oswald, W.W., Saenger, C., Anderson, R.S., Bailey, H.L., Clegg, B., Gajewski, K., Sheng Hu, F., Jones, M.C., Massa, C., Routson, C.C., Werner, A., Wooller, M.J., Yu, Z., 2016. Holocene climate changes in eastern Beringia (NW North America) — a systematic review of multi-proxy evidence. *Quat. Sci. Rev.* 147, 312–339. <https://doi.org/10.1016/j.quascirev.2015.10.021>.
- Krammer, K., Lange-Bertalot, H., 1986–1991. *Bacillariophyceae Band 2/2*. Gustav Fischer Verlag, Stuttgart, pp. 1–4.
- Krawiec, A.C.L., Kaufman, D.S., 2014. Holocene storminess inferred from sediments of two lakes on Adak Island, Alaska. *Quat. Res. (Tokyo)* 82, 73–84. <https://doi.org/10.1016/j.yqres.2014.02.007>.
- Krawiec, A.C.L., Kaufman, D.S., Vaillencourt, D.A., 2013. Age models and tephrostratigraphy from two lakes on Adak Island, Alaska. *Quat. Geochronol.* 18, 41–53. <https://doi.org/10.1016/j.jqageo.2013.07.002>.
- Labeyrie, L.D., 1974. New approach to surface seawater palaeotemperatures using ¹⁸O/¹⁶O ratios in silica of diatom frustules. *Nature* 248, 40–42. <https://doi.org/10.1038/248040a0>.
- Lachniet, M.S., Lawson, D.E., Stephen, H., Sloat, A.R., Patterson, W.P., 2016. Isoscapes of ¹⁸O and ²H reveal climatic forcings on Alaska and Yukon precipitation. *Water Resour. Res.* 52 (8), 6575–6586. <https://doi.org/10.1002/2016WR019436>.
- Lamb, A.L., Brewer, T.S., Leng, M.J., Sloane, H.J., Lamb, H.F., 2007. A geochemical method for removing the effect of tephra on lake diatom oxygen isotope records. *J. Paleolimnol.* 37, 499–516. <https://doi.org/10.1007/s10933-006-9034-5>.
- Larsen, C.F., Burgess, E., Arendt, A.A., O'neel, S., Johnson, A.J., Kienholz, C., 2015. Surface melt dominates Alaska glacier mass balance. *Geophys. Res. Lett.* 42 (14), 5902–5908. <https://doi.org/10.1002/2015GL064349>.
- Leclerc, A.J., Labeyrie, L., 1987. Temperature dependence of the oxygen isotopic fractionation between diatom silica and water. *Earth Planet. Sci. Lett.* 84 (1), 69–74. [https://doi.org/10.1016/0012-821X\(87\)90177-4](https://doi.org/10.1016/0012-821X(87)90177-4).
- Leng, M.J., Barker, P.A., 2006. A review of the oxygen isotope composition of lacustrine diatom silica for paleoclimate reconstruction. *Earth Sci. Rev.* 75, 5–27. <https://doi.org/10.1016/j.earscirev.2005.10.001>.
- Leng, M.J., Sloane, H.J., 2008. Combined oxygen and silicon isotope analysis of biogenic silica. *J. Quat. Sci.* 23, 313–319. <https://doi.org/10.1002/jqs.1177>.
- Leng, M., Barker, P., Greenwood, P., Roberts, N., Reed, J., 2001. Oxygen isotope analysis of diatom silica and authigenic calcite from Lake Pinarbasi, Turkey. *J. Paleolimnol.* 25 (3), 343–349. <https://doi.org/10.1023/A:1011169832093>.
- Lepskaia, E.V., Jewson, D.H., Usoltseva, M.V., 2010. *Aulacoseira subarctica* in Kurilskoye Lake, Kamchatka: a deep, oligotrophic lake and important Pacific salmon nursery. *Diatom Res.* 25 (2), 323–335. <https://doi.org/10.1080/0269249X.2010.9705853>.
- Lotter, A.F., Bigler, C., 2000. Do diatoms in the Swiss Alps reflect the length of ice-cover? *Aquat. Sci.* 62 (2), 125–141. <https://doi.org/10.1007/s000270050002>.
- Lotter, A.F., Pienitz, R., Schmidt, R., 2010. Diatoms as indicators of environmental change in subarctic and alpine regions. In: Smol, J.P., Stoermer, E.F. (Eds.), *The Diatoms: Application for the Environmental and Earth Sciences*. Cambridge University Press, Cambridge.
- Mackay, A.W., Swann, G.E.A., Brewer, T.S., Leng, M.J., Morley, D.W., Piotrowska, N., Rioual, P., White, D., 2011. A reassessment of late glacial–Holocene diatom oxygen isotope record from Lake Baikal using a geochemical mass-balance approach. *J. Quat. Sci.* 26, 627–634. <https://doi.org/10.1002/jqs.1484>.
- Mantua, N.J., Hare, S.R., Zhang, Y., Wallace, J.M., Francis, R.C., 1997. A Pacific interdecadal climate oscillation with impacts on salmon production. *Bull. Am. Meteorol. Soc.* 78, 1069–1079. [https://doi.org/10.1175/1520-0477\(1997\)078<1069:APICOW>2.0.CO;2](https://doi.org/10.1175/1520-0477(1997)078<1069:APICOW>2.0.CO;2).
- Marcott, S.A., Shakun, J.D., Clark, P.U., Mix, A.C., 2013. A reconstruction of regional and global temperature for the past 11 300 years. *Science* 339, 1198–1201. <https://doi.org/10.1126/science.1228026>.
- Max, L., Riethdorf, J.-R., Tiedemann, R., Smirnova, M., Lembke-Jene, L., Fahl, K., Nürnberg, D., Matul, A., Mollenhauer, G., 2012. Sea surface temperature variability and sea-ice extent in the subarctic northwest Pacific during the past 15,000 years. *Paleoceanography* 27, PA3213. <https://doi.org/10.1029/2012PA002292>.
- Mayewski, P.A., Rohling, E.E., Stager, J.C., Karlén, K.A., Maasch, W., Meeker, L.D., Meyerson, E.A., Gasse, F., van Krevelin, S., Holmgren, K., Lee-Thorp, J., Rosqvist, G., Rack, F., Staubwasser, M., Schneider, R.R., Steiger, E.J., 2004. Holocene climate variability. *Qual. Res.* 62, 243–255. <https://doi.org/10.1016/j.yqres.2004.07.001>.
- Meyer, H., Chaplign, B., Hoff, U., Nazarova, L., Diekmann, B., 2015. Oxygen isotope composition of diatoms as late Holocene climate proxy at two-Yurts-lake, central Kamchatka, Russia. *Global Planet. Change* 134, 118–128. <https://doi.org/10.1016/j.gloplacha.2014.04.008>.
- Minoshima, K., Kawahata, H., Ikehara, K., 2007. Changes in biological production in the mixed water region (MWR) of the northwestern North Pacific during the last 27 kyr. *Palaeogeogr. Palaeoclimatol. Palaeoecol.* 254, 430–447. <https://doi.org/10.1016/j.palaeo.2007.06.022>.
- Mock, C.J., Bartlein, P.J., Anderson, P.M., 1998. Atmospheric circulation patterns and spatial climatic variations in Beringia. *Int. J. Climatol.* 10, 1085–1104. [https://doi.org/10.1002/\(SICI\)1097-0088\(199808\)18:10<1085::AID-JOC305>3.0.CO;2-K](https://doi.org/10.1002/(SICI)1097-0088(199808)18:10<1085::AID-JOC305>3.0.CO;2-K).
- Morley, D.W., Leng, M.J., Mackay, A.W., Sloane, H.J., Rioual, P., Battarbee, R.W., 2004. Cleaning of lake sediment samples for diatom oxygen isotope analysis. *J. Paleolimnol.* 31 (3), 391–401. <https://doi.org/10.1023/B:JOPL.0000021854.70714.6b>.
- Nazarova, L., de Hoog, V., Hoff, U., Dirksen, O., Diekmann, B., 2013. Late Holocene climate and environmental changes in Kamchatka inferred from the subfossil chironomid record. *Quat. Sci. Rev.* 67, 81–92. <https://doi.org/10.1016/j.quascirev.2013.01.018>.
- NOAA, 2017. National Oceanic and Atmospheric Administration. National Climatic Data Centre. <https://www.ncdc.noaa.gov/land-based-station-data>.
- Rehfeld, K., Münch, T., Ho, S.L., Laepple, T., 2018. Global patterns of declining

- temperature variability from the last glacial maximum to the Holocene. *Nature* 554 (7692), 356–359. <https://doi.org/10.1038/nature25454>.
- Renssen, H., Seppä, H., Heiri, O., Goosse, H., Fichefet, T., 2009. The spatial and temporal complexity of the Holocene thermal maximum. *Nat. Geosci.* 2, 411–414. <https://doi.org/10.1038/ngeo513>.
- Renssen, H., Seppä, H., Crosta, X., Goosse, H., Roche, D.M., 2012. Global characterization of the Holocene thermal maximum. *Quat. Sci. Rev.* 48, 7–19. <https://doi.org/10.1016/j.quascirev.2012.05.022>.
- Rioual, P., Andrieu-Ponel, V., Rietti-Shati, M., Battarbee, R.W., de Beaulieu, J.L., Cheddadi, R., Reille, M., Svobodova, H., Shemesh, A., 2001. High-resolution record of climate stability in France during the last interglacial period. *Nature* 413 (6853), 293–296. <https://doi.org/10.1038/35095037>.
- Rioual, P., Andrieu-Ponel, V., de Beaulieu, J.L., Reille, M., Svobodova, H., Battarbee, R.W., 2007. Diatom responses to limnological and climatic changes at ribains maar (French Massif central) during the Eemian and early würm. *Quat. Sci. Rev.* 26 (11), 1557–1609. <https://doi.org/10.1016/j.quascirev.2007.03.009>.
- Roberts, S., Jones, V.J., Allen, J.R., Huntley, B., 2015. Diatom response to mid-Holocene climate in three small Arctic lakes in northernmost Finnmark. *Holocene* 25 (6), 911–920. <https://doi.org/10.1177/0959683615572853>.
- Rodionov, S.N., Bond, N.A., Overland, J.E., 2007. The Aleutian Low, storm tracks, and winter climate variability in the Bering Sea. *Deep Sea Res. II* 54, 2560–2577. <https://doi.org/10.1016/j.dsr2.2007.08.002>.
- Rosqvist, G., Jonsson, C., Yam, R., Karlén, W., Shemesh, A., 2004. Diatom oxygen isotopes in pro-glacial lake sediments from northern Sweden: a 5000 year record of atmospheric circulation. *Quat. Sci. Rev.* 23 (7), 851–859. <https://doi.org/10.1016/j.quascirev.2003.06.009>.
- Rühland, K., Priesnitz, A., Smol, J.P., 2003. Paleolimnological evidence from diatoms for recent environmental changes in 50 lakes across Canadian Arctic treeline. *Arctic Antarct. Alpine Res.* 35 (1), 110–123. [https://doi.org/10.1657/1523-0430\(2003\)035\[0110:PEFDFR\]2.0.CO;2](https://doi.org/10.1657/1523-0430(2003)035[0110:PEFDFR]2.0.CO;2).
- Rühland, K., Paterson, A.M., Smol, J.P., 2008. Hemispheric-scale patterns of climate-related shifts in planktonic diatoms from North American and European lakes. *Global Change Biol.* 14 (11), 2740–2754. <https://doi.org/10.1111/j.1365-2486.2008.01670.x>.
- Saros, J.E., Anderson, N.J., 2015. The ecology of the planktonic diatom *Cyclotella* and its implications for global environmental change studies. *Biol. Rev.* 90 (2), 522–541. <https://doi.org/10.1111/brv.12120>.
- Savoskul, O.S., 1999. Holocene glacier advances in the headwaters of sredniaya Avacha, Kamchatka, Russia. *Qual. Res.* 52, 14–26. <https://doi.org/10.1006/qres.1999.2051>.
- Schiff, C.J., Kaufman, D.S., Wolfe, A.P., Dodd, J., Sharp, Z., 2009. Late Holocene storm-trajectory changes inferred from the oxygen isotope composition of lake diatoms, south Alaska. *J. Paleolimnol.* 41, 189–208. <https://doi.org/10.1007/s10933-008-9261-z>.
- Smol, J.P., Wolfe, A.P., Birks, H.J.B., Douglas, M.S., Jones, V.J., Korhola, A., Pienitz, R., Rühland, K., Sorvari, S., Antoniades, D., Brooks, S.J., 2005. Climate-driven regime shifts in the biological communities of arctic lakes. *Proc. Natl. Acad. Sci. Unit. States Am.* 102 (12), 4397–4402. <https://doi.org/10.1073/pnas.0500245102>.
- Solomina, O.N., Bradley, R.S., Hodgson, D.A., Ivy-Ochs, S., Jomelli, V., Macintosh, A.N., Nesje, A., Owen, L.A., Wanner, H., Wiles, G.C., Young, N.E., 2015. Holocene glacier fluctuations. *Quat. Sci. Rev.* 111, 9–34. <https://doi.org/10.1016/j.quascirev.2014.11.018>.
- Solovieva, N., Klimaschewski, A., Self, A.E., Jones, V.J., Andrén, E., Andreev, A.A., Hammarlund, D., Lepskaya, E.V., Nazarova, L., 2015. The Holocene environmental history of a small coastal lake on the north-eastern Kamchatka Peninsula. *Global Planet. Change* 134, 55–66. <https://doi.org/10.1016/j.gloplacha.2015.06.010>.
- Spaulding, S.A., Lubinski, D.J., Potapova, M., 2017. Diatoms of the United States. <http://westerndiatoms.colorado.edu>.
- Streletskiy, D.A., Tananaev, N.I., Opel, T., Shiklomanov, N.I., Nyland, K.E., Streletskaia, I.D., Shiklomanov, A.I., 2015. Permafrost hydrology in changing climatic conditions: seasonal variability of stable isotope composition in rivers in discontinuous permafrost. *Environ. Res. Lett.* 10 (9), 095003. <https://doi.org/10.1088/1748-9326/10/9/095003>.
- Sundqvist, H.S., Kaufman, D.S., McKay, N.P., Balascio, N.L., Briner, J.P., Cwynar, L.C., Sejrup, H.P., Seppä, H., Subetto, D.A., Andrews, J.T., Axford, Y., 2014. Arctic Holocene proxy climate database—new approaches to assessing geochronological accuracy and encoding climate variables. *Clim. Past* 10 (4), 1605–1631. <https://doi.org/10.5194/cp-10-1605-2014>.
- Swann, G.E.A., Patwardhan, S.V., 2011. Application of Fourier Transform Infrared Spectroscopy (FTIR) for assessing biogenic silica sample purity in geochemical analyses and palaeoenvironmental research. *Clim. Past* 7, 65–74. <https://doi.org/10.5194/cp-7-65-2011>.
- TDX, 2013. TDX Power - Adak Reconnaissance Study. Hatchet. <http://akenergyinventory.org/hyd/SSH-2013-0004.pdf>.
- ter Braak, C.J.F., Prentice, I.C., 1988. A theory of gradient analysis. *Adv. Ecol. Res.* 18, 271–317. [https://doi.org/10.1016/S0065-2504\(03\)34003-6](https://doi.org/10.1016/S0065-2504(03)34003-6).
- Trenberth, K.E., Hurrell, J.W., 1994. Decadal atmosphere-ocean variations in the Pacific. *Clim. Dynam.* 9, 303–319. <https://doi.org/10.1007/BF00204745>.
- USGS, 2017. USGS Landsat 8 Images. Available at: <https://landsat.gsfc.nasa.gov/>.
- Vachula, R.S., Chipman, M.L., Hu, F.S., 2017. Holocene climatic change in the Alaskan Arctic as inferred from oxygen-isotope and lake-sediment analyses at Wahoo Lake. *Holocene* 27 (4), 1–14. <https://doi.org/10.1177/0959683617702230>.
- Walker, M., Berhelhammer, M., Björck, S., Cwynar, L.C., Fisher, D.A., Long, A.J., Lowe, J.J., Newnham, R.M., Rasmussen, S.O., Weis, H., 2012. Formal subdivision of the Holocene series/epoch: a discussion paper by a working group of INTIMATE (Integration of ice-core, marine and terrestrial records) and the sub-commission on quaternary stratigraphy (International commission on stratigraphy). *J. Quat. Sci.* 27, 649–659. <https://doi.org/10.1002/jqs.2565>.
- Wang, L., Lu, H., Liu, J., Gu, Z., Mingram, J., Chu, G., Li, J., Rioual, P., Negendank, J.F., Han, J., Liu, T., 2008. Diatom-based inference of variations in the strength of Asian winter monsoon winds between 17,500 and 6000 calendar years BP. *J. Geophys. Res. Atmos.* 113, D2101. <https://doi.org/10.1029/2008JD010145>.
- Welker, J.M., 2000. Isotopic ($\delta^{18}\text{O}$) characteristics of weekly precipitation collected across the USA: an initial analysis with application to water source studies. *Hydrol. Process.* 14 (8), 1449–1464. [https://doi.org/10.1002/1099-1085\(20000615\)14:8<1449::AID-HYP993>3.0.CO;2-7](https://doi.org/10.1002/1099-1085(20000615)14:8<1449::AID-HYP993>3.0.CO;2-7).
- Wiles, G., D'Arrigo, R., Villalba, R., Calkin, P., Barclay, D.J., 2004. Century-scale solar variability and Alaskan temperature change over the past millennium. *Geophys. Res. Lett.* 31, L15203. <https://doi.org/10.1029/2004GL020050>.
- Zander, P.D., Kaufman, D.S., Kuehn, S.C., Wallace, K.L., Anderson, R.S., 2013. Early and late Holocene glacial fluctuations and tephrostratigraphy, Cabin Lake, Alaska. *J. Quat. Sci.* 28, 761–771. <https://doi.org/10.1002/jqs.2671>.
- Zhang, Y., Renssen, H., Seppä, H., Valdes, P.J., 2017. Holocene temperature evolution in the Northern Hemisphere high latitudes—Model-data comparisons. *Quat. Sci. Rev.* 173, 101–113. <https://doi.org/10.1016/j.quascirev.2017.07.018>.